A&A 609, A11 (2018)
DOI: 10.1051/0004-6361/201731645

Astronomy & Astrophysics

Cosmic flow around local massive galaxies

Olga G. Kashibadze* and Igor D. Karachentsev

Special Astrophysical Observatory of the Russian Academy of Sciences Nizhnij Arkhyz, 369167 Karachay-Cherkessia, Russia
e-mail: phiruzi@gmail.com

Received 24 July 2017 / Accepted 19 September 2017

ABSTRACT

Aims. We use accurate data on distances and radial velocities of galaxies around the Local Group, as well as around 14 other massive nearby groups, to estimate their radius of the zero-velocity surface, R_0, which separates any group against the global cosmic expansion.
Methods. Our R_0 estimate was based on fitting the data to the velocity field expected from the spherical infall model, including effects of the cosmological constant. The reported uncertainties were derived by a Monte Carlo simulation.
Results. Testing various assumptions about a location of the group barycentre, we found the optimal estimates of the radius to be 0.91 ± 0.05 Mpc for the Local Group, and 0.93 ± 0.02 Mpc for a synthetic group stacked from 14 other groups in the Local Volume. Under the standard *Planck* model parameters, these quantities correspond to the total mass of the group $\sim(1.6 \pm 0.2) \times 10^{12}\ M_\odot$. Thus, we are faced with the paradoxical result that the total mass estimate on the scale of $R_0 \approx (3\text{–}4)R_{\rm vir}$ is only 60% of the virial mass estimate. Anyway, we conclude that wide outskirts of the nearby groups do not contain a large amount of hidden mass outside their virial radius.

Key words. galaxies: groups: general – galaxies: groups: individual: Local Group

1. Introduction

Any overdense region in the Universe is driven by the competition between its self-gravity and the cosmic expansion, and therefore can be characterized by an idealized zero-velocity surface that separates these zones. de Vaucouleurs (1958, 1964, 1972) presupposed systematic deviations from linearity in the velocity-distance relation and interpreted these deviations as a local phenomenon caused by the Virgo complex. The expected effect has only subsequently been supported by observations. Peebles (1976) found the virgocentric infall signal using the field galaxy data available at that time (Sandage & Tammann 1975).

Lynden-Bell (1981) and Sandage (1986) focussed on the Local Group of galaxies. They showed that, in the simplest case of the spherically symmetric system in the empty Universe with $\Lambda = 0$, the radius of the zero-velocity surface R_0 and the total mass of the group M_T^0 are related as

$$M_T^0 = (\pi^2/8G) \times R_0^3 \times T_0^{-2}, \quad (1)$$

where G is the gravitational constant and T_0 is the age of the Universe (Lynden-Bell 1981; Sandage 1986). In the standard cosmological ΛCDM model, where $\Omega_{\rm m}$ is the mean cosmic density of matter and H_0 the Hubble parameter, the relation between R_0 and M_T becomes

$$M_T = (\pi^2/8G) \times R_0^3 \times H_0^2/f^2(\Omega_{\rm m}), \quad (2)$$

where the dimensionless parameter

$$f(\Omega_{\rm m}) = (1-\Omega_{\rm m})^{-1} - \frac{\Omega_{\rm m}}{2}(1-\Omega_{\rm m})^{-\frac{3}{2}} \cosh^{-1}\left(\frac{2}{\Omega_{\rm m}} - 1\right) \quad (3)$$

changes in the range from 1 to 2/3 while varying $\Omega_{\rm m}$ from 0 to 1. Taking the *Planck* model parameters $\Omega_{\rm m} = 0.315$, $\Omega_\lambda = 0.685$ and $H_0 = 67.3$ km s^{-1} Mpc^{-1} (Planck Collaboration XVI 2014), we obtain the relation

$$(M_T/M_\odot)_{0.315} = 1.95 \times 10^{12}(R_0/{\rm Mpc})^3, \quad (4)$$

which is by 1.50 times more than the classical estimate from Eq. (1).

This method was sucessfully applied to determine masses of the Local Group (Ekholm et al. 2001; Karachentsev et al. 2002, 2009; Teerikorpi et al. 2005), M81 group (Karachentsev & Kashibadze 2006), CenA group (Karachentsev et al. 2006), as well as the Virgo cluster (Tully & Shaya 1984; Karachentsev & Nasonova 2010; Karachentsev et al. 2014) and the Fornax cluster (Nasonova et al. 2011).

It is important to stress that the R_0 method estimates the total mass of a group independently of mass estimates based on virial motions. Notably, the corresponding total mass M_T is confined on the linear scale of R_0, which is three to four times as large as the virial radius of a group or cluster, $R_{\rm vir}$.

The implementation of the R_0 method became possible with wholesale measurements of distances to nearby galaxies from luminosities of the red giant branch stars (TRGB) with accuracy of ∼5% attainable by the *Hubble* Space Telescope. In the Local Volume, limited to 11 Mpc, there are about a thousand known galaxies; most of these galaxies have measured radial velocities with a typical accuracy less than 5 km s^{-1}. About one-third of the Local Volume population already has accurate TRGB distance estimates. The compilation of observational data on these objects is presented in the Updated Nearby Galaxy Catalog (Karachentsev et al. 2013) and its latest electronic version[1] (Kaisina et al. 2012). For a typical galaxy of the Local Volume with a distance of ∼6 Mpc, the TRGB distance error of ∼300 kpc is comparable with a virial radius of the group, thus its location can be confidently fixed relative to the group centroid and

* F.k.a. Nasonova.

[1] http://sao.ru/lv/lvgdb/

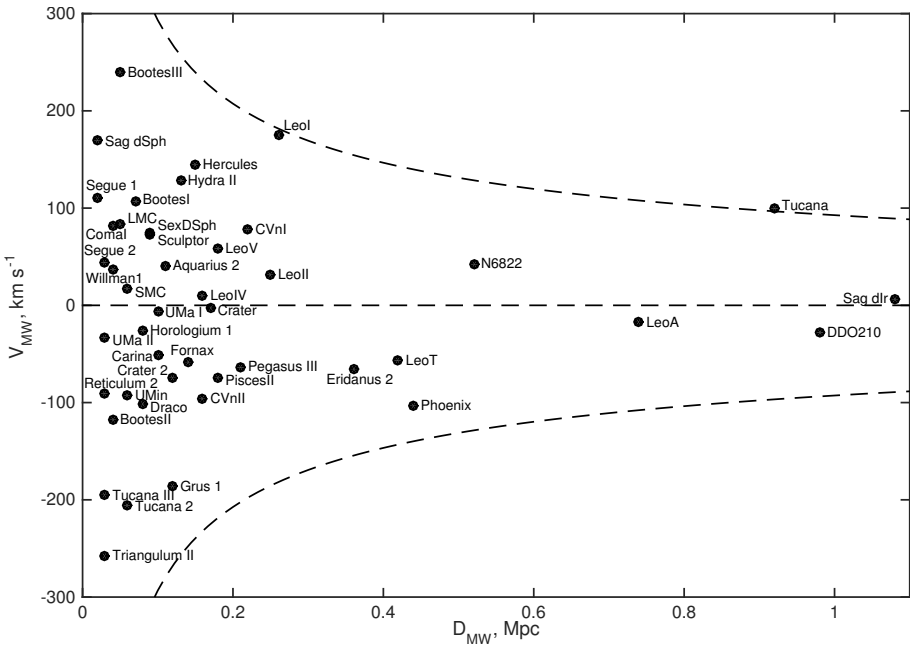

Fig. 1. Distribution of 45 Milky Way satellites by their spatial distances and radial velocities relative to the Milky Way. Dashed lines correspond to the parabolic velocity for a point mass of $1 \times 10^{12}\ M_\odot$.

zero velocity surface. Other methods of secondary importance are the Tully & Fisher (1977) relation distances or the brightest stars distances with an accuracy of ∼(20−30)%, which do not provide an opportunity to determine R_0 value even for the nearest groups.

Below we use the most complete data on distances and radial velocities of the Local Volume galaxies to estimate the zero-velocity radius around the local massive galaxies.

2. Galaxy motions around the Milky Way and M31

The recent surveys of large sky areas (Abazajian et al. 2009; Tonry et al. 2012; Koposov et al. 2015) led to the discovery of new Milky Way (MW) dwarf satellites with low luminosities and extremely low surface brightnesses. The recent overview by McConnachie (2012) reports 29 MW satellites with measured radial velocities and accurate distances. In recent years, this list has been expanded up to 45 objects. The corresponding data are presented in Table 1. The table columns contain (1) galaxy name; (2) equatorial coordinates J2000.0; and (3) tidal index,

$$TI = \max[\log(M_n^*/D_n^3)] - 10.96, \quad n = 1, 2, \ldots N, \tag{5}$$

distinguishing the most significant galaxy (main disturber = MD) among N neighbouring galaxies, whose tidal force dominates the remaining galaxies with masses M_n^* and spatial separations D_n. The constant, −10.96, is chosen in such a way that $TI = 0$ corresponds to a significant neighbour located on the zero velocity surface with $TI < 0$ galaxies ranked as isolated. Finally, Col. (4) lists the main disturber name, Col. (5) distance to a galaxy in Mpc, and Cols. (6, 7) radial velocity of a galaxy (in km s^{-1}) relative to the Sun and relative to the MW centre with apex parameters adopted in NASA Extragalactic Database (NED). References to the used values of distances and velocities of galaxies are presented in the Local Volume Galaxies Database[2].

The distribution of 45 satellites of the MW by their Galactocentric distances and radial velocities is shown in Fig. 1. The dashed lines correspond to the parabolic velocity for a point mass of $1 \times 10^{12}\ M_\odot$. The velocity distribution of satellites looks symmetrical relative to the MW centre, although two satellites with near-parabolic velocities – Tucana and LeoI – are close to the upper escape limit. Three MW satellites, Sag dIr, DDO 210, and Tucana with distances $D \sim 1$ Mpc and negative Θ_1, belong to field galaxies. However, the MW is dynamically the most significant neighbour for each of these.

Specialized searches for faint satellites in the outskirts of the spiral galaxy M31 in the Andromeda constellation (Ibata et al. 2007, 2014; Martin et al. 2009) has proved to be notably productive. While the sample by McConnachie (2012) included 23 satellites, now their number is roughly doubled amounting up to 44. The data on these satellites are presented in Table 2, where the first six columns have the same meaning as in Table 1. The seventh column of Table 2 contains spatial distances of satellites (in Mpc) relative to M31, while eighth and ninth list the projected separation of satellites in the sky (in Mpc) and their differential radial velocities relative to M31 (in km s^{-1}). Aside from dwarf galaxies, we tabulate also the data on eight distant globular clusters from PAndAS survey (Huxor et al. 2014) with measured radial velocities. Their spatial distances still remain unknown, and we set them equal to 0.78 Mpc.

The distribution of 44 + 8 test particles by their differential radial velocities and projected separations relative to M31 is presented in Fig. 2. The dashed lines also mean the parabolic velocity for a point mass of $1 \times 10^{12}\ M_\odot$. Similar to the MW case, the distribution of M31 satellites by their relative velocities seems to be very symmetrical; two satellites – And XIV and And XII – have near-parabolic velocities that are close to the lower escape limit.

3. Orbital masses of the Milky Way and M31

For a massive galaxy surrounded by small satellites, the orbital mass estimate is expressed as

$$M_{\rm orb} = (32/3\pi) \times (1 - 2e^2/3)^{-1} \times G^{-1} \times \langle \Delta V^2 \times R_p \rangle, \tag{6}$$

where $\langle \Delta V^2 \times R_p \rangle$ is the mean product of squared radial velocity difference of a satellite with its projected distance from the main galaxy and e is the orbit eccentricity (Karachentsev & Kudrya 2014). This relation is obtained under

[2] http://sao.ru/lv/lvgdb/

Table 1. Milky Way companions with $TI > -0.5$.

Name	RA (2000.0) Dec hh mm ss dd mm ss	TI	MD	D_{MW} Mpc	V_h km s^{-1}	V_{MW} km s^{-1}
(1)	(2)	(3)	(4)	(5)	(6)	(7)
SMC	005238.0 −724801	3.32	LMC	0.06	158	17
Sculptor	010009.4 −334233	2.79	MWay	0.09	105	72
Phoenix	015106.3 −442641	0.73	MWay	0.44	−13	−103
Triangulum II	021317.4 +361042	3.97	MWay	0.03	−382	−257
Segue 2	021916.0 +201031	3.83	MWay	0.03	−39	44
Fornax	023954.7 −343133	2.19	MWay	0.14	29	−59
Horologium 1	025531.7 −540708	2.94	MWay	0.08	113	−26
Reticulum 2	033542.1 −540257	4.15	MWay	0.03	64	−91
Eridanus 2	034421.1 −433159	1.00	MWay	0.36	76	−66
LMC	052334.6 −694522	3.56	MWay	0.05	278	84
Carina	064136.7 −505758	2.63	MWay	0.10	224	−52
UMa II	085130.0 +630748	3.92	MWay	0.03	−116	−33
Leo T	093453.4 +170305	0.77	MWay	0.42	39	−57
Leo A	095926.4 +304447	0.03	MWay	0.74	24	−17
Segue 1	100703.2 +160425	4.32	MWay	0.02	206	111
Leo I	100826.9 +121829	1.37	MWay	0.26	283	175
Sex dSph	101303.0 −013652	2.74	MWay	0.09	227	75
UMa I	103452.8 +515512	2.59	MWay	0.10	−55	−7
Willman 1	104921.0 +510300	3.76	MWay	0.04	−12	36
Leo II	111329.2 +220917	1.45	MWay	0.25	86	32
Leo V	113109.6 +021312	1.89	MWay	0.18	173	59
Leo IV	113257.0 −003200	2.05	MWay	0.16	132	10
Crater	113615.8 −105240	1.96	MWay	0.17	148	−2
Crater 2	114914.4 −182447	2.50	MWay	0.12	88	−74
Hydra II	122142.1 −315907	2.29	MWay	0.13	303	129
Coma I	122659.0 +235415	3.74	MWay	0.04	98	82
CVn II	125710.0 +341915	2.04	MWay	0.16	−129	−96
CVn I	132803.5 +333321	1.60	MWay	0.22	31	78
Bootes III	135707.4 +264630	3.67	MWay	0.05	198	240
Bootes II	135800.0 +125100	3.86	MWay	0.04	−117	−117
Bootes I	140000.0 +143000	3.25	MWay	0.07	99	106
UMin	150911.3 +671252	3.27	MWay	0.06	−255	−93
Hercules	163102.0 +124730	2.19	MWay	0.15	45	145
Draco	172001.4 +575434	2.94	MWay	0.08	−296	−101
Sag dSph	185503.1 −302842	5.36	MWay	0.02	140	169
Sag dIr	192959.0 −174041	−0.44	MWay	1.08	−79	7
NGC 6822	194457.7 −144811	0.52	MWay	0.52	−57	43
DDO 210	204651.8 −125053	−0.31	MWay	0.98	−140	−28
Pegasus III	222424.2 +052436	1.73	MWay	0.21	−223	−63
Aquarius 2	223355.5 −091939	2.56	MWay	0.11	−71	41
Tucana	224149.0 −642512	−0.24	MWay	0.92	194	99
Tucana 2	225155.1 −583408	3.46	MWay	0.06	−129	−205
Grus 1	225642.4 −500948	2.45	MWay	0.12	−140	−186
Pisces II	225831.0 +055709	1.88	MWay	0.18	−226	−75
Tucana III	235636.0 −593600	3.90	MWay	0.03	−102	−195

the assumption of uniformly random orientation of satellite orbits relative to the line of sight. With the typical eccentricity value of $\langle e^2 \rangle = 1/2$ (Barber et al. 2014) the relation (6) becomes

$$M_{orb} = (16/\pi) \times G^{-1} \times \langle \Delta V^2 \times R_p \rangle. \quad (7)$$

Applying Eq. (7) to the assembly of the MW and M31 satellites, we get values for orbital masses $M_{orb}(MW) = 1.51 \times 10^{12}\ M_\odot$ and $M_{orb}(M31) = 1.69 \times 10^{12}\ M_\odot$. Since in the case of MW satellites we observe their 3D distances, then project distances, the orbital mass estimation should be reduced by a factor of $(\pi/4)$ yielding $M_{orb}(MW) = 1.18 \times 10^{12}\ M_\odot$. Hence, the ratio of mass estimates for these two galaxies reaches

$$M_{orb}(MW)/M_{orb}(M31) \simeq 0.70. \quad (8)$$

This value is quite close to the ratio $M_{orb}(MW)/M_{orb}(M31) = 0.82$ obtained by Karachentsev & Kashibadze (2006) from a minimum value for scatter of peculiar velocities with respect to the Hubble regression line, while varying the centroid position between the MW and M31.

A comparison of the derived total masses of the MW and M31, their combined mass, and the mass ratio with other mass estimates in the recent literature is presented in Table 3. These estimates were based on kinematics of satellites and globular clusters assuming that the MW and M31 haloes follow the standard NFW profile or fit the kinematics of high-velocity stars and blue horizontal branch stars. Our present measurements are in good agreement with the median values given in the last line of Table 3. An essential part of the mismatch between the different estimates in Table 3 may arise from the observed orbital anisotropy of the MW and M31 satellites (Ibata et al. 2013; Pawlowski et al. 2014) and from the uncertain dynamical status of two MW satellites, Leo I and Tucana, and the two

Table 2. M31 companions.

Name	RA (2000.0) Dec hh mm ss dd mm ss	TI	MD	D_{MW} Mpc	V_h km s^{-1}	D_{M31} Mpc	R_p Mpc	ΔV km s^{-1}
(1)	(2)	(3)	(4)	(5)	(6)	(7)	(8)	(9)
WLM	000158.1 −152740	−0.01	M31	0.98	−122	0.88	0.75	14
And XVIII	000214.5 +450520	0.72	M31	1.31	−332	0.51	0.11	−14
And XIX	001932.1 +350237	2.21	M31	0.93	−111	0.16	0.10	187
IC 10	002024.5 +591730	1.58	M31	0.79	−346	0.26	0.25	−32
And XXVI	002345.6 +475458	2.58	M31	0.76	−261	0.12	0.10	50
Cetus	002611.0 −110240	0.27	M31	0.79	−87	0.71	0.69	55
And XXV	003008.9 +465107	3.01	M31	0.81	−108	0.09	0.08	200
NGC 147	003311.6 +483028	2.55	M31	0.76	−193	0.12	0.10	115
And III	003533.8 +362952	2.80	M31	0.75	−346	0.10	0.07	−54
Cas III	003559.4 +513335	2.28	M31	0.78	−372	0.15	0.14	−64
And XXX	003634.9 +493848	2.28	NGC 185	0.68	−141	0.18	0.11	166
And XVII	003707.0 +441920	2.95	M31	0.74	−251	0.09	0.04	51
And XXVII	003727.1 +452313	3.47	M31	0.83	−535	0.06	0.06	−232
NGC 185	003858.0 +482010	2.03	M31	0.66	−203	0.18	0.10	102
NGC 205	004022.5 +414111	4.68	M31	0.80	−221	0.02	0.01	77
M 32	004242.1 +405159	4.38	M31	0.79	−202	0.03	0.01	93
M31	004244.5 +411609	2.79	NGC 205	0.78	−296	0.00	0.00	0
And I	004540.0 +380214	2.77	M31	0.73	−376	0.10	0.04	−86
And XI	004620.0 +334805	2.43	M31	0.73	−419	0.14	0.10	−137
And XII	004727.0 +342229	2.82	M31	0.83	−556	0.10	0.09	−274
Bol 520	005042.4 +325459	1.79	M31	0.63	−312	0.22	0.12	−34
And XIV	005135.0 +294149	2.04	M31	0.73	−481	0.18	0.16	−211
And XIII	005151.0 +330016	2.55	M31	0.84	−195	0.12	0.12	82
And IX	005252.8 +431200	3.65	M31	0.79	−216	0.05	0.04	77
PAndAS-48	005928.2 +312910	2.31	M31	0.82	−250	0.15	0.14	19
And XVI	005929.8 +322236	1.32	M31	0.52	−385	0.32	0.13	−114
LGS 3	000355.0 +215306	1.37	M31	0.65	−286	0.30	0.27	−44
IC 1613	000447.8 +020800	0.64	M31	0.76	−232	0.54	0.53	−59
And X	000633.7 +444816	1.90	M31	0.63	−164	0.20	0.08	124
And V	001007.1 +473741	2.64	M31	0.81	−403	0.11	0.11	−113
And XV	001418.7 +380703	2.64	M31	0.76	−323	0.11	0.09	−49
And II	001629.8 +332509	1.82	M31	0.65	−194	0.21	0.14	69
And XXIV	001830.0 +462158	1.65	M31	0.60	−128	0.24	0.11	156
And XXII	002740.0 +280525	1.75	M31	0.79	−127	0.23	0.22	116
And XXIII	002921.8 +384308	2.24	M31	0.73	−243	0.15	0.13	23
M 33	003350.8 +303937	1.63	M31	0.93	−182	0.25	0.20	63
Perseus I	030123.6 +405918	1.14	M31	0.79	−326	0.36	0.35	−116
And XXVIII	223241.2 +311258	1.04	M31	0.65	−331	0.39	0.38	−3
Lac I	225816.3 +411728	1.50	M31	0.76	−198	0.27	0.26	137
Cas dSph	232631.8 +504032	1.73	M31	0.82	−307	0.23	0.22	24
Pegasus	232834.1 +144448	0.73	M31	0.97	−184	0.50	0.42	89
Peg dSph	235146.4 +243510	1.48	M31	0.82	−345	0.28	0.27	−55
And XXI	235447.7 +422815	2.42	M31	0.86	−361	0.14	0.12	−43
And XXIX	235855.6 +304520	1.87	M31	0.73	−194	0.21	0.19	106
PAndAS −04	000442.9 +472142	2.5	M31	0.78	−397	...	0.12	−79
PAndAS −05	000524.1 +435535	2.8	M31	0.78	−183	...	0.10	132
PAndAS −50	010150.6 +481819	2.7	M31	0.78	−323	...	0.11	−29
PAndAS −56	012303.5 +415511	2.7	M31	0.78	−239	...	0.10	36
PAndAS −57	012747.5 +404047	2.6	M31	0.78	−186	...	0.12	84
PAndAS −58	012902.1 +404708	2.5	M31	0.78	−167	...	0.12	103
PAndAS −01	235712.0 +433308	2.6	M31	0.78	−333	...	0.12	−15
PAndAS −02	235755.6 +414649	2.6	M31	0.78	−266	...	0.11	50

M31 satellites, And XIV and And XII. Excluding these objects reduces the mass estimates by 14−15% in both cases.

4. Hubble flow around the Local Group

The proximate velocity field around the Local Group was considered in most detail by Karachentsev & Kashibadze (2006) and Karachentsev et al. (2009). For a sample of 30 galaxies with TRGB distances from 0.7 to 3.0 Mpc with respect to the Local Group centre, it was shown that the Hubble flow is characterized by the local Hubble parameter $H_{loc} = (78 \pm 2)$ km s^{-1} Mpc^{-1}, the radial velocity dispersion $\sigma_v \simeq 25$ km s^{-1}, and the radius of zero-velocity surface $R_0 = (0.96 \pm 0.03)$ Mpc. The minimal value of σ_v corresponded to the barycentre position of $D_c = (0.55 \pm 0.05)D_{M31} = 0.43$ Mpc, determining the mass ratio of $M_{MW}/M_{M31} \simeq 0.8$ stated above.

In that approach, we considered the so-called minor attractor model, illustrated by the upper panel of Fig. 3. Here, a galaxy

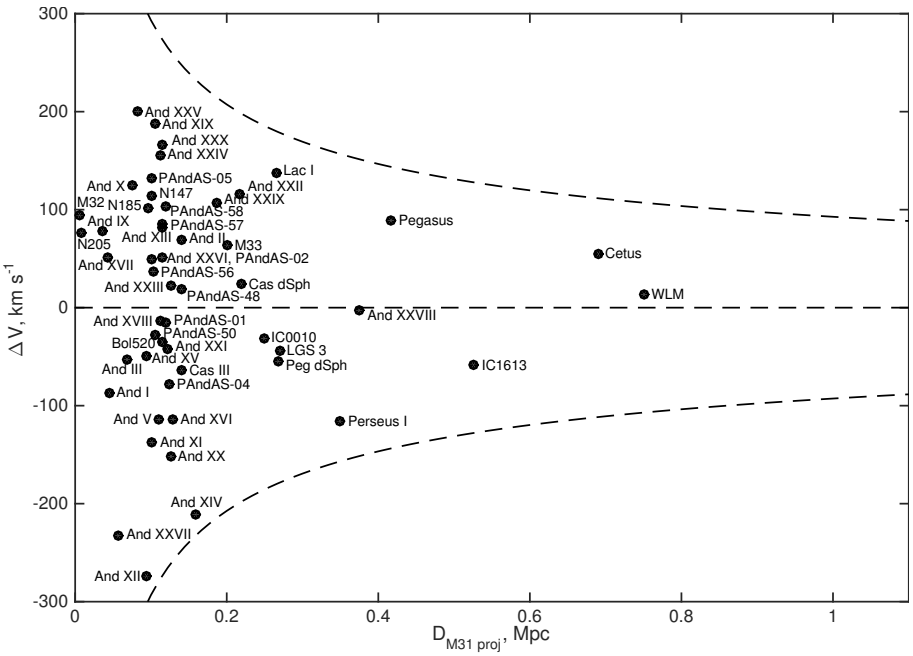

Fig. 2. Distribution of 52 test particles by their differential radial velocities and projected distances from M31. Dashed lines correspond to the parabolic velocity for a point mass of $1 \times 10^{12}\ M_\odot$.

Table 3. Total mass estimates for the Milky Way and M31 (in $10^{12}\ M_\odot$).

M(MW)	M(M31)	M(MW+M31)	M(M31)/M(MW)	Reference
0.75 ± 0.25	...	...	...	(1)
...	...	3.2 ± 0.6	...	(2)
...	1.35 ± 0.20	...	...	(3)
0.80 ± 0.50	1.70 ± 0.30	2.5 ± 0.6	2.3	(4)
0.7 ± 0.4	...	...	...	(5)
1.6 ± 0.4	1.8 ± 0.5	3.4 ± 0.6	1.1	(6)
1.35 ± 0.47	1.76 ± 0.33	3.1 ± 0.6	1.3	(7)
1.2 ± 0.4	0.9 ± 0.3	2.1 ± 0.5	0.75	(8)
0.70 ± 0.51	1.39 ± 0.26	2.1 ± 0.6	2.0	(9)
...	...	2.6 ± 0.4	...	(10)
1.30 ± 0.30	...	...	...	(11)
1.02 ± 0.76	...	...	...	(12)
1.55 ± 0.35	...	...	...	(13)
2.84	1.65	4.5	0.58	(14)
1.18 ± 0.18	1.69 ± 0.25	2.9 ± 0.3	1.4	(15)
1.2	1.7	2.9	1.3	median

References. (1) Deason et al. (2012); (2) van der Marel et al. (2012); (3) Veljanoski et al. (2013); (4) Diaz et al. (2014); (5) Bhattacharjee et al. (2014); (6) Shull (2014); (7) Karachentsev & Kudrya (2014); (8) Penarrubia et al. (2014); (9) Sofue (2015); (10) Penarrubia et al. (2016); (11) McMillan (2017); (12) Patel et al. (2017); (13) Fragione & Loeb (2017); (14) Peebles (2017); (15) present paper.

group with centre, C, is separated by a distance, D_c, from the observer, O, and moves away along the line of site with the velocity, V_c. In the outskirts of the group there is a galaxy, G, with distance, D_g, and radial velocity, V_g. If the angle between C and G is θ, then their mutual separation is expressed as

$$R^2 = D_g^2 + D_c^2 - 2D_g \times D_c \times \cos\theta, \quad (9)$$

and the projected differential velocity is given by

$$V_{gc} = V_g \times \cos\lambda - V_c \times \cos\mu, \quad (10)$$

where $\mu = \lambda + \theta$, and

$$\tan\lambda = D_c \times \sin\theta / (D_g - D_c \times \cos\theta). \quad (11)$$

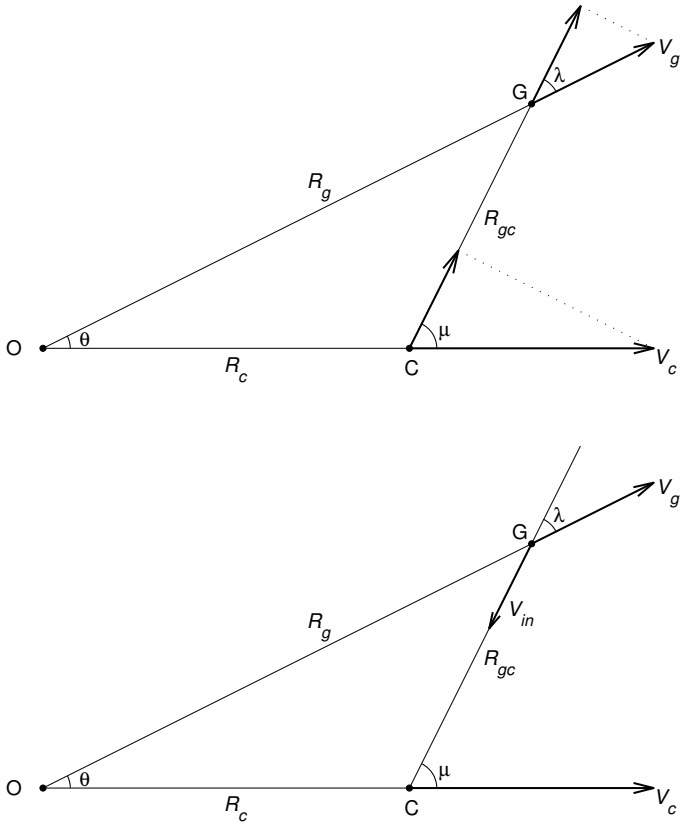

Fig. 3. Models of major and minor attractor. O represents an observer, C represents the centre of a galaxy group, and G represents a test particle (a galaxy).

In this scheme we assumed peculiar velocities of galaxies in the vicinity of a group to be small compared with velocities of the regular Hubble flow.

Yet, there is another possibility, which is the major attractor case (see lower panel of Fig. 3); this case is characterized by predominating infall towards the centre of a group or a cluster.

Table 4. Isolated galaxies around the Local Group.

Name	D_{MW} Mpc	V_h km s^{-1}	R_c Mpc	V_c^{mi} km s^{-1}	V_c^{ma} km s^{-1}	TI	MD	λ deg
(1)	(2)	(3)	(4)	(5)	(6)	(7)	(8)	(9)
WLM	0.98	−122	0.83	−10	−7	−0.01	M31	27
NGC 404	2.98	−50	2.53	205	205	−0.76	Maffei2	1
KKs3	2.00	316	2.24	103	109	−1.25	MWay	11
KKH 37	3.44	11	3.17	217	221	−0.04	M81	6
UGC 4879	1.37	−25	1.34	25	33	−0.63	M31	19
Leo A	0.74	24	0.93	−47	−53	0.03	MWay	29
Sex B	1.43	300	1.71	94	101	−0.82	MWay	13
NGC 3109	1.34	403	1.73	94	96	−0.33	Antlia	9
Sex A	1.45	324	1.78	78	82	−0.83	MWay	11
Leo P	1.73	262	1.95	120	128	−1.07	MWay	12
NGC 3741	3.22	229	3.27	255	262	−0.69	M81	8
DDO 99	2.65	251	2.76	247	255	−0.62	NGC 4214	9
IC 3104	2.36	429	2.73	159	162	−1.12	NGC 4945	6
DDO 125	2.61	206	2.69	242	251	−0.94	M81	10
DDO 147	3.01	331	3.14	342	350	−0.60	NGC 4214	8
GR 8	2.19	217	2.48	128	132	−1.37	MWay	9
UGC 8508	2.67	56	2.66	176	184	−0.80	M81	10
DDO 181	3.10	214	3.19	278	285	−0.87	NGC 4736	8
DDO 183	3.31	188	3.41	247	253	−0.79	NGC 4736	8
KKH 86	2.61	287	2.93	198	202	−1.38	NGC 5128	7
UGC 8833	3.25	221	3.37	273	280	−0.89	NGC 4736	8
KK 230	2.21	63	2.34	120	127	−1.34	M81	11
DDO 187	2.30	160	2.51	171	178	−1.44	MWay	10
DDO 190	2.83	150	2.88	258	267	−1.18	M81	9
ESO 274–01	2.79	524	3.20	327	329	−0.51	NGC 5128	4
KKR 25	1.91	−79	1.84	126	137	−0.98	M31	14
IC 4662	2.55	302	2.87	131	135	−1.24	NGC 5128	7
NGC 6789	3.55	−140	3.28	153	156	−1.32	M81	6
Sag dIr	1.08	−79	1.19	20	29	−0.44	MWay	22
DDO 210	0.98	−140	0.98	12	22	−0.31	MWay	27
IC 5152	1.96	122	2.08	70	77	−1.20	NGC 253	12
KK 258	2.24	92	2.18	151	160	−0.91	NGC 253	12
Tucana	0.92	194	1.14	61	77	−0.24	MWay	22
UGCA 438	2.22	62	2.15	101	108	−0.48	NGC 55	12
KKH 98	2.58	−132	2.14	171	171	−0.93	M31	2

If V_i is the infall velocity than

$$V_g = V_c \times \cos\theta - V_i \times \cos\lambda, \quad (12)$$

and the velocity of a galaxy relative to the group centre is expressed as

$$V_i = [V_c \times \cos\theta - V_g]/\cos\lambda. \quad (13)$$

Evidently the difference between these two models would be insignificant if the galaxy lays almost strictly behind ($\lambda \simeq 0$) or in front ($\lambda \simeq 180°$) of the group centre.

The last few years astronomers have detected some new dwarf galaxies in the vicinity of the Local Group (KKs3, LeoP, and KK258) and measured their accurate TRGB distances and radial velocities. For some galaxies (KKR25 and Tucana), old inexact values of radial velocities were corrected and distances were refined. This circumstance has motivated us to redefine parameters of the local Hubble flow.

To reduce the role of virial motions, we excluded galaxies with $TI > 0$ from consideration; thus, the MW and M31 satellites with distances $D_{MW} < 0.8$ Mpc were consequently excluded. The data on the rest field galaxies with $D_{MW} < 3.5$ Mpc are presented in Table 4. The columns of Table 4 contain (1) galaxy name; (2) distance (in Mpc) from the Milky Way; (3) heliocentric radial velocity (in km s^{-1}); (4) distance from the Local Group barycentre located at $D_c = 0.43$ Mpc; (5, 6) velocity (in km s^{-1}) relative to the barycentre in the case of minor and major attractor, respectively; (7) tidal index; (8) the main disturber name; and (9) λ in degrees (see Fig. 3).

The distribution of 35 isolated galaxies by distances and velocities relative to the Local Group barycentre for the case of minor attractor is presented in the upper panel of Fig. 4. As shown in the Table 4 data, only 14 galaxies of 35 have the MW or M31 as the main disturber; they are denoted by solid circles. With reference to these objects, the zone affected gravitationally by the Local Group reaches $R_c \simeq 2.5$ Mpc, while more distant field galaxies are influenced by other massive neighbours of the Local Group, such as M81, NGC 253, and NGC 5128.

According to Peirani & de Freitas Pacheco (2008), Falco et al. (2014), and Penarrubia & Fattahi (2017), the radial velocity profile around the spherically symmetrical group or cluster can be expressed as

$$V(R) = H_0 \times R - H_0 \times R_0 \times (R_0/R)^{1/2}, \quad (14)$$

where R_0 is the radius of the zero-velocity surface to be found. The solid line in Fig. 4 corresponds to Eq. (14) with parameters defined from the least squares method, $R_0 = 0.95 \pm 0.03$ Mpc, $H_0 = 90 \pm 2$ km s^{-1} Mpc^{-1}, and $\sigma_v = 42$ km s^{-1}. The errors of R_0 and H_0 parameters were estimated using the Monte Carlo method, assuming that distance errors for galaxies are distributed

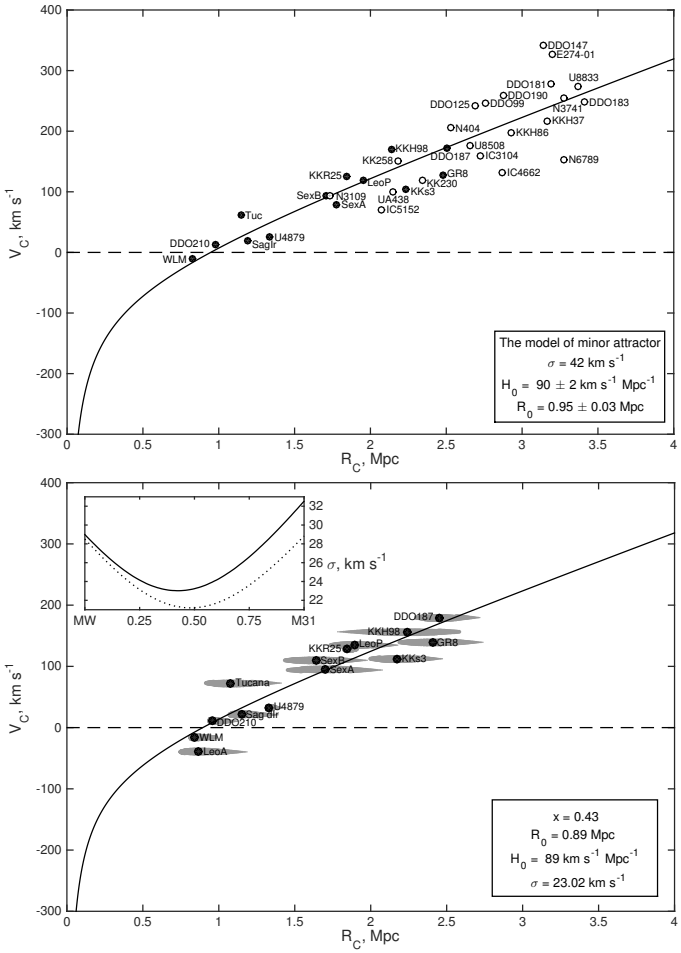

Fig. 4. Distribution of isolated galaxies by distances and velocities relative to the Local group barycentre assuming the minor attractor model. *Upper panel*: barycentre position locates at $x = D_c/D_{M31} = 0.55$ towards the M31. The solid circles indicate galaxies that have the MW or M31 as the main disturber. *Lower panel*: Hubble flow around the LG at the barycentre position of $x = D_c/D_{M31} = 0.43$. The grey wedges trace the companion positions under different x, where their thin end corresponds to the barycentre coinciding with M31. Solid and dotted lines in the insert indicate the velocity dispersion as a function of x with and without the Leo A, respectively.

normally with a typical value of ∼5%. The peculiar velocity dispersion in the upper panel of Fig. 4 is contributed mostly by distant galaxies, which are disturbed by the neighbouring groups. Considering the only 14 galaxies in the zone affected gravitationally by the Local Group, we obtain the following parameters for the surrounding Hubble flow: $R_0 = 0.85 \pm 0.03$ Mpc, $H_0 = 79 \pm 3$ km s^{-1} Mpc^{-1}, and $\sigma_v = 23$ km s^{-1}. In the major attractor model, these parameters vary slightly, since λ values for these 14 galaxies are small (see the last column in Table 4).

Three parameters, i.e. R_0, H_0, and σ_v, characterizing the local cosmic expansion, moderately depend on the position of the LG barycentre. Above, we used the barycentre location at the distance of $D_c = 0.55 D_{M31} = 0.43$ Mpc, corresponding to the mass ratio of $M_{M31}/M_{MW} = 1.2$. This ratio matches well with the medians in Table 3. However, Penarrubia et al. (2014) found that the minimal scatter of nearby galaxies within 3 Mpc around the LG is achieved with $M_{M31}/M_{MW} = 0.75$. The authors have concluded that their analysis rules out models in which M31 is more massive than our Galaxy with about 95% confidence. To check this statement, we calculated σ_v for 14 nearest

Table 5. Parameters of the local Hubble flow as a function of the LG barycentre position.

$x = D_C/D_{M31}$	0.10	0.20	0.30	0.40	0.50	0.60	0.70	0.80	0.90
M_{M31}/M_{MW}	0.11	0.25	0.43	0.67	1.00	1.50	2.33	4.00	9.00
σ_v, km s^{-1}	26.7	24.9	23.6	23.1	23.4	24.2	25.7	27.7	30.0
R_0, Mpc	0.83	0.85	0.87	0.89	0.91	0.93	0.95	0.97	0.99

isolated galaxies as a function of the position of the LG barycentre $x = D_c/D_{M31}$ on the line connecting the MW with M31. The data on σ_v and R_0 are presented in Table 5. The lower panel of Fig. 4 shows the local Hubble diagram for 14 galaxies at various M31-to-MW mass ratios. Each galaxy is drawn by grey wedge with caliber inversely related to the dispersion σ_v at given barycentre position; thus its thinner end indicates the barycentre position at M31. The insert in the figure shows the velocity scatter of galaxies respect to the best-fitting regression line. The solid and dotted lines in the insert represent the behaviour of σ_v for a case of included or excluded Leo A, respectively. This dwarf galaxy is a marginally isolated object with the tidal index $TI = +0.03$. The derived minimums of these two lines fix the M31-to-MW mass ratio near 0.7 and 1.0, respectively, not allowing a firm assessment of which galaxy mass is dominated. Over the range of $M_{M31}/M_{MW} = [1/3-3]$ the value of the zero velocity radius is changing within $R_0 = 0.86-0.96$ Mpc. Thus, the observed coldness of the local Hubble flow leads us to measure the radius of the sphere separating the Local Group from the global cosmic expansion with ∼5% error. According to (4), the radius $R_0 = 0.91 \pm 0.05$ Mpc yields the total mass estimate for the Local Group $M_T = (1.5 \pm 0.2) \times 10^{12}\ M_\odot$ with an unprecedented accuracy, although this quantity lies below all values of M(MW+M31) in Table 3. The mismatch becomes slightly less dramatic when the *Planck* model parameters in (4) replace the WMAP parameters as follows: $\Omega_m = 0.24$, $\Omega_\lambda = 0.76$, and $H_0 = 73$ km s^{-1} Mpc^{-1} (Spergel 2007); this increases the coefficient in (4) from 1.95 to 2.12.

As noted by Chernin et al. (2004), the actual deviation of the binary shape of the Local Group from the spherical symmetry produces a minor bias in the R_0 and mass estimate. According to N-body simulations by Penarrubia et al. (2014), neglecting the quadrupole potential overestimates the Local Group mass up to ∼30%.

5. Other massive galaxies in the Local volume

Considering the Hubble flow around other giant galaxies of the Local Volume, we selected 15 galaxies with stellar masses $M^* > 3 \times 10^{10}\ M_\odot$ and accurate distances. Their overview is presented in Table 6 with objects ranging by their distances from the observer. For each of these 15 galaxies, surrounded by a suite of satellites, the second most massive member of its group is also indicated. In some cases, i.e. M31 and the Milky Way, NGC 5128 (CenA) and NGC 5236, Maffei 2, and IC 342, the second galaxy is comparable in mass with the first galaxy and acts itself as the centre of a dynamically separated subgroup.

The columns of Table 6 contains (1) galaxy name; (2, 3) its supergalactic coordinates; (4) the galaxy distance from the MW; (5) its radial velocity relative to the Local Group centroid; (6) logarithmic stellar mass; (7) logarithmic orbital mass according to Karachentsev & Kudrya (2014); (8) number of satellites of the main galaxy with measured radial velocities and accurate distances.

Table 6. Giant galaxies in the Local Volume.

Galaxy	SGL deg	SGB deg	D_{MW} Mpc	V_{LG} km s^{-1}	lg M^* $M_\odot$	lg M_{orb} $M_\odot$	N_{sat} (V, D)
(1)	(2)	(3)	(4)	(5)	(6)	(7)	(8)
M31	336.19	12.55	0.78	−29	10.79	12.49	90
M Way	...	...	0.01	−65	10.70		
M81	41.12	0.59	3.70	104	10.95	12.69	22
M 82	40.72	1.05	3.61	328	10.59		
NGC 5128	159.75	−5.25	3.68	310	10.89	12.89	28
NGC 5236	147.93	0.99	4.90	307	10.86		
Maffei 2	359.58	0.83	3.48	214	10.86	12.51	3
IC 342	10.60	0.37	3.28	244	10.60		
NGC 253	271.57	−5.01	3.70	276	10.98	12.18	7
NGC 247	275.92	−3.73	3.72	216	9.50		
NGC 4826	95.61	6.13	4.41	365	10.49	10.78	4
DDO 154	90.13	6.90	4.04	354	7.59		
NGC 4736	76.24	9.50	4.41	352	10.56	12.43	16
NGC 4449	72.30	6.18	4.27	249	9.68		
M 101	63.58	22.61	6.95	378	10.79	12.17	6
NGC 5474	64.30	22.93	6.98	424	9.21		
NGC 4258	68.74	5.55	7.66	506	10.92	12.50	7
NGC 4242	70.28	4.81	7.9:	568	9.47		
NGC 5055	76.20	14.25	9.04	562	11.00	12.49	0
NGC 4460	71.58	6.48	9.59	551	9.66		
NGC 4594	126.69	−6.68	9.30	894	11.30	13.45	0
NGC 4597	121.05	−5.12	10.1:	912	9.48		
NGC 6744	208.10	10.38	9.51	706	10.91	11.72	4
NGC 6684	205.81	9.11	8.7:	720	10.39		
NGC 3115	112.40	−42.86	9.68	439	10.95	12.54	0
P 4078671	114.10	−45.34	9.38	378	7.95		
NGC 2683	55.87	−33.42	9.82	334	10.81	12.13	2
KK 69	55.64	−33.09	9.16	418	7.27		
NGC 3379	93.64	−25.85	11.32	774	10.92	13.23	3
NGC 3368	94.29	−26.41	10.42	740	10.83		

Aside from the galaxies presented in Table 6, the Local Volume contains another two massive galaxies – NGC 2903 ($\log M^* = 10.82$) and NGC 6946 ($\log M^* = 10.76$). But their distances measured from the luminosity of brightest stars are not yet sufficiently accurate. In total, the 15 giant galaxies have about 500 satellites in their suites, but, as shown in the last column of Table 6, only 102 satellites outside the Local Group have accurate estimates of distances and velocities. Among the second most massive members of 15 groups, three galaxies – NGC 4242, NGC 4597 and NGC 6684 – have Tully-Fisher distances with accuracy of ~20% (denoted with column signs). In 11 of 15 groups, the main galaxy exceeds its satellites twice or more in mass, allowing us to estimate its halo mass from the orbital motions. This approach is not worthwhile in the case of the rich group Leo I, where NGC 3379, NGC 3368, and several other bright members have compatible luminosities.

Despite the great efforts to measure highly accurate TRGB distances of nearby galaxies from *Hubble* Space Telescope data, many neighbouring groups stay still poorly explored. For example, in the outskirts of giant galaxies NGC 4594 (Sombrero), NGC 5055, and NGC 3115, no satellites have reliable distance estimates.

6. Cosmic flow around the synthetic (stacked) nearby group

Seeking to use as much information as possible about companion motions around the nearby massive galaxies outside their virial zones, we combined the data on companions of various galaxies into the single synthetic group. To be included into the consolidated group, a galaxy should satisfy the following four conditions: (1) a companion has accurate estimates of distance and radial velocities; (2) the companion distance from the main galaxy, R_{MG}, is less than 3.5 Mpc; (3) the companion belongs to field galaxies, having $TI < 0$; and (4) the companion has a proper aspect, when its position angle λ between the vector of companion radial velocity and the line joining it with the main galaxy (see Fig. 3) lays within $\lambda < 45°$ or $\lambda > 135°$.

These conditions are satisfied for 66 galaxies of the Local Volume; the corresponding data are presented in Table 7. Its

Table 7. Isolated galaxies around the nearby group centres.

Main gal.	Name	R_C Mpc	V_{mi} km s^{-1}	V_{ma} km s^{-1}	TI	MD	λ deg
(1)	(2)	(3)	(4)	(5)	(6)	(7)	(8)
M81	UGC 04879	2.40	141	147	−0.63	M31	153
M81	UGC 06456	1.26	−38	−86	−0.31	M81	35
M81	NGC 3738	2.16	150	170	−1.01	M81	33
M81	UGC 06757	1.37	51	42	−0.41	M81	40
M81	UGC 07242	2.06	56	48	−0.40	N4605	24
M81	NGC 4236	1.13	17	−15	−0.16	M81	44
M81	NGC 4605	2.36	131	138	−1.07	M101	29
M81	DDO165	1.71	56	41	−0.64	N4236	39
M81	UGC 08245	1.54	14	−27	−0.58	M81	40
NGC 5128	NGC 3621	3.50	219	204	−1.68	N4594	34
NGC 5128	ESO 320-014	2.66	134	100	−0.68	N3621	38
NGC 5128	ESO 379-007	2.07	129	111	−1.04	N5236	45
NGC 5128	ESO 381-018	1.45	81	74	−0.40	N5236	29
NGC 5128	ESO 381-020	1.47	55	39	−0.33	N5236	29
NGC 5128	ESO 443-009	1.97	124	119	−0.53	N5236	24
NGC 5128	KK182	1.80	66	62	−0.67	N5236	16
NGC 5128	ESO 270-017	2.86	282	289	−1.35	N5236	15
NGC 5128	HIPASS J1348-37	1.45	56	54	−0.21	N5236	12
NGC 5128	HIPASS J1351-47	1.80	20	−11	−0.87	N5236	29
NGC 5128	NGC 5408	1.28	0	−25	−0.35	N5236	29
NGC 5128	ESO 223-009	2.78	142	120	−1.42	N5236	33
Maffei2	UGC 01281	3.00	215	223	−1.20	N784	37
Maffei2	KK17	2.97	220	238	−0.96	N784	41
Maffei2	NGC 0784	3.25	240	254	−1.30	U1281	37
Maffei2	KKH18	2.45	207	243	−1.17	Maffei2	42
Maffei2	KKH34	1.80	110	106	−0.65	M81	39
N253	WLM	2.76	288	298	−0.01	M31	161
N253	NGC 0045	3.02	259	260	−1.05	N24	10
N253	PiscesA	3.49	278	292	−1.68	N253	40
N253	NGC 0059	1.35	163	174	−0.37	N253	23
N253	DDO226	1.24	136	138	−0.27	N253	9
N253	UGCA438	1.76	178	221	−0.48	N55	136
N4826	AGC 749241	1.32	65	59	−0.73	N4656	20
N4826	GR8	2.26	227	230	−1.37	MW	165
N4826	DDO187	2.34	202	207	−1.44	MW	144
N4736	NGC 3741	1.47	105	95	−0.69	M81	135
N4736	DDO099	1.87	99	86	−0.62	N4214	153
N4736	UGCA281	1.48	30	12	−0.92	N4258	24
N4736	DDO126	0.76	−64	−136	−0.02	N4736	37
N4736	DDO125	1.80	92	90	−0.94	M81	169
N4736	Arp 211	1.78	146	146	−0.86	N4258	9
N4736	DDO147	1.42	−4	−13	−0.60	N4214	164
N4736	NGC 5023	1.72	141	141	−0.89	M101	13
N4736	UGC 08508	1.94	172	183	−0.80	M81	144
N4736	DDO181	1.44	73	59	−0.87	N4736	149
N4736	DDO183	1.36	107	109	−0.79	N4736	136
N4736	KK230	2.36	220	235	−1.34	M81	148
N4736	DDO190	1.91	116	85	−1.18	M81	135
M101	LV J1157+5638	3.00	190	215	−0.80	N4258	45
M101	NGC 4068	3.07	131	98	−0.48	N4736	137
M101	MCG +09-20-131	2.82	161	167	−0.43	N4736	137
M101	UGC 07298	3.14	149	136	−0.35	N4736	142
M101	NGC 4736	3.07	87	12	−0.13	N4449	136
M101	NGC 5204	2.44	49	40	−0.88	N4736	162
M101	NGC 5238	2.49	43	37	−0.41	N4736	166
M101	KKH87	1.97	97	96	−0.81	N5194	11
M101	DDO194	1.29	15	−4	−0.10	N5585	150
N4258	KK109	3.23	270	275	−0.32	N4736	164
N4258	MCG +06-27-017	3.05	185	180	−0.22	N4395	151
N4258	NGC 4395	3.25	222	225	−0.12	N4736	146
N4258	NGC 4707	1.38	−9	−66	−0.45	N4258	143
N4258	NGC 4861	3.17	371	464	−0.57	N5055	37
N6744	IC 4710	2.06	139	137	−0.99	N6684	158
N6744	IC 4870	1.00	4	−40	−0.22	N6744	142
N2683	AGC182595	1.61	27	12	−0.78	N2683	144
N3379	DDO088	3.20	328	329	−0.45	N3627	174

Table 8. Parameters of the Hubble flow around the nearby synthetic group under various assumptions.

Case	Minor attractor			Major attractor		
	H_0 km s^{-1} Mpc^{-1}	σ_v km s^{-1}	R_0 Mpc	H_0 km s^{-1} Mpc^{-1}	σ_v km s^{-1}	R_0 Mpc
(1)	(2)	(3)	(4)	(5)	(6)	(7)
Main galaxy (MG)	76	62	0.83	80	84	0.93
MG-normalized	80	65	0.71	82	89	0.76
Barycentre (BC)	85	57	0.93	85	84	1.03
BC-normalized	88	66	0.76	95	85	0.93

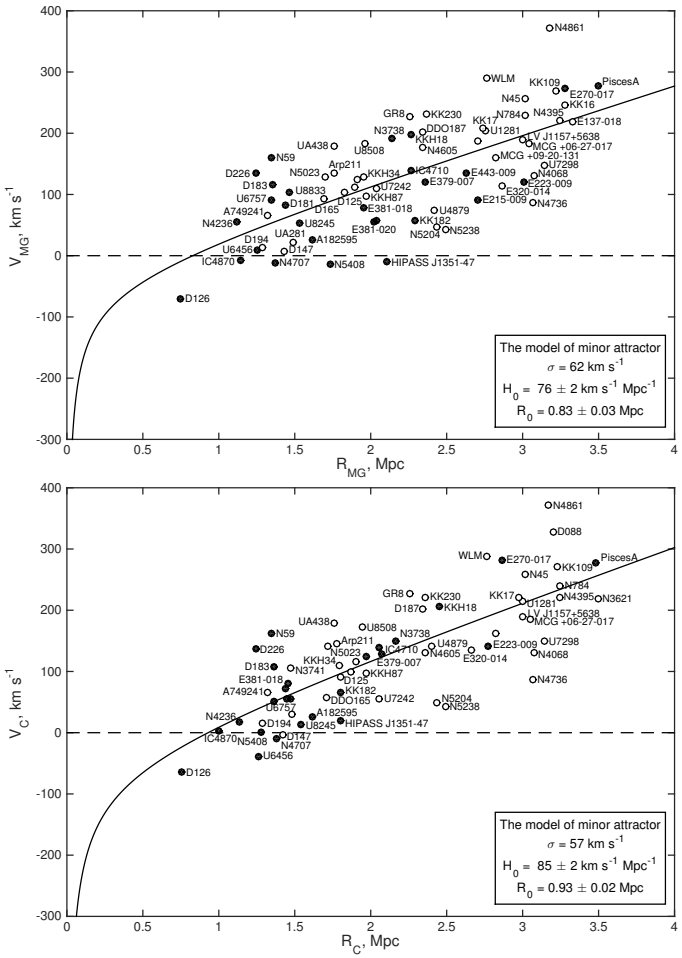

Fig. 5. Hubble diagram for the synthetic group of the Local Volume, assuming the minor attractor model. *Upper panel*: distances and velocities of satellites are calculated relative to the main galaxy in a group. *Lower panel*: distances and velocities of satellites are calculated relative to the barycentre of a pair of the most massive galaxies in each group.

columns contain: (1) name of the main galaxy acting as the centre of its suite; (2) name of a companion galaxy; (3) companion galaxy distance from the group barycentre; (4, 5) companion galaxy velocity relative to the group barycentre in the case of minor or major attractor; (6, 7) tidal index of the galaxy and the name of its main disturber; and (8) position angle of the companion as indicated in Fig. 3.

The Hubble diagram for the synthetic group of the Local Volume for the minor attractor model with distances and velocities calculated relative to the main galaxy is shown in the upper panel of Fig. 5. The cosmic flow around the synthetic group is characterized by the Hubble parameter $H_0 = (76 \pm 2)$ km s^{-1}/Mpc, velocity dispersion $\sigma_v = 62$ km s^{-1}, and radius of the zero velocity surface $R_0 = 0.83 \pm 0.03$ Mpc. As one can see, the radius R_0 turned out to be quite small, corresponding to the effective mass of the synthetic group of $\sim 1.1 \times 10^{12}\ M_\odot$. To estimate how various factors influence R_0, we constructed another series of Hubble diagrams. An alternative Hubble diagram with distances and velocities calculated relative to the group barycentre rather than from the main galaxy itself is presented in the lower panel of Fig. 5. The barycentre is supposed to lie between the two most massive galaxies of each group given in Table 6. In this case the local Hubble parameter is $H_0 = (85 \pm 2)$ km s^{-1} Mpc, peculiar velocity dispersion $\sigma_v = 57$ km s^{-1}, and radius R_0 reaches $R_0 = 0.93 \pm 0.02$ Mpc.

As follows from the data on Table 6, the nearby galaxy groups differ substantially in their stellar and virial masses, M^* and $M_{\rm orb}$, which can lead to a systematic bias in the averaged R_0 estimate. To verify this effect, we normalized distances of companions around each group to its individual radius R_0, assuming $R_0 \propto M_*^{1/3}$ or $R_0 \propto M_{\rm orb}^{1/3}$. After that we did not find any decrease in peculiar velocity dispersion in the synthetic Hubble diagram.

The resulting values of H_0, σ_v, and R_0 parameters for all discussed cases are presented in Table 8; i.e. distances and velocities calculated relative to the main galaxy or group barycentre and the minor or major attractor model. These data allow us to conclude, first, that changing a model from a minor attractor to major attractor increases the R_0 estimate and causes a significant increment in dispersion, and, second, that accounting for the second most massive galaxy in a group leads to a notable growth of the R_0 estimate.

7. Discussion

As our estimates suggest, galaxies in the infall zone between the virial radius and the R_0 are relatively small in number, ~15%. This circumstance, inherent for the Local Group and for other nearby groups, opts for estimating R_0 value within minor attractor model. The low value of peculiar velocity dispersion resulting in this case is also an oblique argument for such a choice.

The second most massive galaxy plays an essential role in the kinematics of several nearby groups, often forming a dynamical subsystem. So, deciding on a barycentre of the two most bright galaxies as the reference point for distances and velocities of companions seems to be more preferable than the main galaxy itself. Hence, we adopt the value of 0.93 ± 0.02 Mpc as the optimal estimate for R_0 radius of the cumulative group (see the lower panel of Fig. 5). The corresponding mass is $\log(M_T/M_\odot) = 12.20$ with a formal error of ~0.04 dex. Averaging orbital mass estimates from Table 6 and considering the representation of each group in the Hubble diagram, we obtain the mean logarithmic mass $\log(M_{\rm orb}/M_\odot) = 12.42 \pm 0.07$. So, the mass of the synthetic group derived from outer motions of surrounding galaxies turned out to be ~60% of the expected

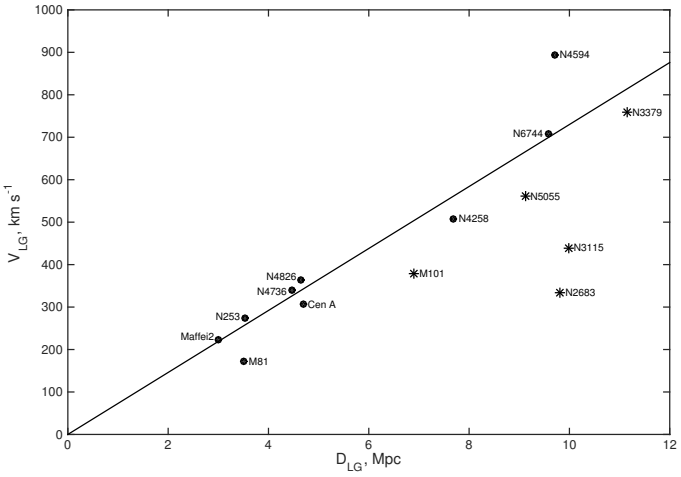

Fig. 6. Distribution of barycentres of 15 nearby groups by their radial velocities and distances from the Local Group centre. The solid line corresponds to the regular Hubble flow with Hubble parameter H_0 = 73 km s^{-1} Mpc^{-1}.

mass from inner orbital motions of satellites. A probable source of this discrepancy was discussed by Chernin et al. (2013) and Karachentsev & Kudrya (2014).

As noted by Chernin et al. (2013), the estimate of the total mass of a group includes two components, $M_T = M_\mathrm{m} + M_\mathrm{DE}$, where M_m is the mass of dark and baryonic matter and M_DE is the mass, negative in magnitude, which is determined by the dark energy with the density of ρ_DE,

$$M_\mathrm{DE} = (8\pi/3) \times \rho_\mathrm{DE} \times R^3. \quad (15)$$

On the scale of virial radius, the contribution of this component in the group mass does not exceed 1%, but in the sphere of R_0 radius, the role of this kind of a mass defect becomes significant. In the standard ΛCDM model with $\Omega_\mathrm{m} = 0.24$ and $H_0 = 73$ km s^{-1} Mpc^{-1} the contribution of dark energy is

$$(M_\mathrm{DE}/M_\odot) = -0.85 \times 10^{12} \times (R_0/\mathrm{Mpc})^3, \quad (16)$$

i.e. about 30% of the Local Group mass determined by orbital motions. This correction essentially reduces the observed discrepancy between the mass estimates for the Local Group, as well as for other nearby groups, derived via internal (virial) and external galaxy motions.

Another possible explanation might be caused by the existence of unrelaxed (tidal) thin planar structures of satellites seen around the MW and M31 (Kroupa 2014), which are at variance with the assumption of spherical symmetry case.

The peculiar velocity dispersion in the vicinity of the synthetic group, 57 km s^{-1}, is twice as large as in the outskirts of the Local Group. This difference might originate from bulk motions of galaxies, which become perceptible on the scale of ∼5−10 Mpc. A giant galaxy is not necessarily the main disturber for neighbouring field galaxies. Indeed, this is the case for only a portion of companion objects presented in Table 7. Another portion, which are comprised of mostly distant field galaxies (shown by open circles), are gravitationally influenced by a massive galaxy from another neighbouring group.

Figure 6 reproduces the distribution of barycentres of 15 nearby groups listed in Table 5 by distances and radial velocities relative to the Local Group centre. The straight line corresponds to the regular Hubble flow with H_0 = 73 km s^{-1} Mpc^{-1}. Barycentres of the groups with $D_\mathrm{LG} < 6$ Mpc situated in the supergalactic plane (i.e. in the Local Sheet; Tully et al. 2016) demonstrate a small scatter of radial velocities. More distant groups, around M 101, NGC 5055, NGC 2683, NGC 3115, and NGC 3379 at supergalactic latitudes $|SGB| > 10°$ (denoted with asterisks), exhibit negative peculiar velocities about −200 km s^{-1}. These velocities are caused by the observed expansion of the Local Void with an amplitude of ∼260 km s^{-1} (Tully et al. 2016). Also, the group around Sombrero (NGC 4594) is located just near the zero-velocity surface of the Virgo cluster. Its positive peculiar velocity reflects the group fall towards the cluster. Apparently, some portion of these bulk motions manifest themselves as extra peculiar velocities of the Local Volume galaxies in the panels of Fig. 5. Ignoring these non-virial coherent motions may lead to the overestimation of galaxy masses based on the Numerical Action Method (Peebles 2017).

Our conclusion that the peripheral regions of the Local Group and other neighbouring groups do not contain a large amount of dark matter seems to be the most important result of this work. The bulk of mass is concentrated within the virial radius of these groups. The same inference was made for the nearest Virgo cluster (Karachentsev et al. 2014) from the observed infall of galaxies towards the cluster centre. Yet further evidence is provided by Kourkchi & Tully (2017), who have considered infall zones and collapsed cores of halos in the Local Universe.

A review of available observational data on distances and radial velocities of the Local Volume galaxies shows that the population of outskirts of the nearby groups has not yet been covered with highly accurate distance measurements. There are groups, for example around the giant Sombrero galaxy, totally lack reliable distance estimates, even for close probable satellites. The systematical measurements of TRGB distances with the *Hubble* Space Telescope within the Local Volume have the potential to provide meaningful data on the distribution of the dark matter on the scales of ∼1 Mpc.

Acknowledgements. The authors are grateful to Elena Kaisina for updating the Local Volume Galaxies Database (`https://www.sao.ru/lv/lvgdb/`), Dmitry Makarov for the renewed data on galaxy tidal indices, and Brent Tully for reviewing the manuscript and for his helpful comments. This work is supported by the Russian Science Foundation grant No. 14–12–00965.

References

Abazajian, K. N., Adelman-McCarthy, J. K., Agüeros, M. A., et al. 2009, ApJS, 182, 543
Barber, C., Starkenburg, E., Navarro, J. F., et al. 2014, MNRAS, 437, 959
Bhattacharjee, P., Chaudhury, S., & Kundu, S. 2014, ApJ, 785, 63
Chernin, A. D., Karachentsev, I. D., Valtonen, M. J., et al. 2004, A&A, 415, 19
Chernin, A. D., Bisnovatyi-Kogan, G. S., Teerikorpi, P., et al. 2013, A&A, 553, A101
Deason, A. J., Belokurov, V., Evans, N. W., et al. 2012, MNRAS, 425, 2840
de Vaucouleurs, G. 1958, AJ, 63, 253
de Vaucouleurs, G. 1964, AJ, 69, 737
de Vaucouleurs, G. 1972, in External Galaxies and Quasi-Stellar Objects, eds. D. S. Evans, D. Wills, & B. J. Wills (Dordrecht: Reidel), IAU Symp., 44, 353
Diaz, J. D., Koposov, S. E., Irwin, M., et al. 2014, MNRAS, 443, 1688
Ekholm, T., Baryshev, Y., Teerikorpi, P., et al. 2001, A&A, 368, L17
Falco, M., Hansen, S. H., Wojtak, R., et al. 2014, MNRAS, 442, 1887
Fragione, G., & Loeb, A. 2017, New Astron., 55, 32
Huxor, A. P., Mackey, A. D., Ferguson, A. M. N., et al. 2014, MNRAS, 442, 2165
Ibata, R., Martin, N. F., Irwin, M., et al. 2007, ApJ, 671, 1591
Ibata, R. A., Lewis, G. F., Conn, A. R., et al. 2013, Nature, 493, 62
Ibata, R. A., Lewis, G. F., McConnachie, A. W., et al. 2014, ApJ, 780, 128
Kaisina, E. I., Makarov, D. I., & Karachentsev, I. D. 2012, Astrophys. Bull., 67, 115
Karachentsev, I. D., & Kashibadze, O. G. 2006, Astrophysics, 49, 3

Karachentsev, I. D., & Kudrya, Y. N. 2014, AJ, 148, 50
Karachentsev, I. D., & Nasonova, O. G. 2010, MNRAS, 405, 1075
Karachentsev, I. D., Sharina, M. E., Makarov, D. I., et al. 2002, A&A, 389, 812
Karachentsev, I. D., Dolphin, A. E., Tully, R. B., et al. 2006, AJ, 131, 1361
Karachentsev, I. D., Kashibadze, O. G., Makarov, D. I., & Tully, R. B. 2009, MNRAS, 393, 1265
Karachentsev, I. D., Makarov, D. I., & Kaisina, E. I. 2013, AJ, 145, 101
Karachentsev, I. D., Tully, R. B., Wu, Po-Feng, Shaya, E. J., & Dolphin, A. E. 2014, ApJ, 782, 4
Koposov, S. E., Belokurov, V., Torrealba, G., & Wyn, E. N. 2015, ApJ, 805, 130
Kourkchi, E., & Tully, R. B. 2017, ApJ, 843, 16
Kroupa, P. 2014, ArXiv e-prints [arXiv:1409.6302]
Lynden-Bell, D. 1981, Observatory, 101, 111
Martin, N. F., McConnachie, A. W., Irwin, M., et al. 2009, ApJ, 705, 758
McConnachie, A. W. 2012, AJ, 144, 4
McMillan, P. J. 2017, MNRAS, 465, 76
Nasonova, O. G., de Freitas Pacheco, J. A., & Karachentsev, I. D. 2011, A&A, 532, A104
Patel, E., Besla, G., & Mandel, K. 2017, MNRAS, 468, 3428
Pawlowski, M. S., Famaey, B., Jerjen, H., et al. 2014, MNRAS, 442, 2362
Peebles, P. J. E. 1976, ApJ, 205, 318
Peebles, P. J. E. 2017, ArXiv e-prints [arXiv:1705.10683]
Peirani, S., & de Freitas Pacheco, J. A. 2008, A&A, 488, 845
Penarrubia, J., & Fattahi, A. 2017, MNRAS, 468, 1300
Penarrubia, J., Ma, Y. Z., Walker, M. G., & McConnachie, A. W. 2014, MNRAS, 443, 2204
Penarrubia, J., Gomez, F. A., Besla, G., et al. 2016, MNRAS, 456, L54
Planck Collaboration XVI. 2014, A&A, 571, A16
Sandage, A. 1986, ApJ, 307, 1
Sandage, A., & Tammann, G. A. 1975, ApJ, 196, 313
Shull, J. M. 2014, ApJ, 784, 142
Sofue, Y. 2015, PASJ, 67, 75
Spergel, D. N. 2007, ApJS, 170, 377
Teerikorpi, P., Chernin, A. D., & Baryshev, Y. V. 2005, A&A, 440, 791
Tonry, J. L., Stubbs, C. W., Lykke, K. R., et al. 2012, ApJ, 750, 99
Tully, R. B., & Fisher, J. R. 1977, A&A, 54, 661
Tully, R. B., & Shaya, E. J. 1984, ApJ, 281, 31
Tully, R. B., Courtois, H. M., & Sorce, J. G. 2016, AJ, 152, 50
van der Marel, R. P., Fardal, M., Besla, G., et al. 2012, ApJ, 753, 8
Veljanoski, J., Ferguson, A. M. N., Mackey, A. D., et al. 2013, ApJ, 768, L33